

RESEARCH

Open Access



MicroRNA-24-3p targeting Top1 in perirenal fat is involved in circulating inflammation and high cardiovascular disease risk in patients with primary aldosteronism

Xuelin Li^{1,2†}, Min Luo^{3†}, Yanmei Zeng^{1†}, Renyi Zhang^{4†}, Xiaochun Lin¹, Yuejun Du⁵, Wei Zhao⁶, Qijian Feng¹, Minghai Wu¹, Jin Zhang¹, Lei Guo¹, Peili Wu¹, Chuyi Yang¹, Feifei Cai¹, Yuan Wang¹, Yuxuan Hu¹, Huiyun Wang¹, Nannan Liu¹, Lingling Xu² and Meiping Guan^{1*}

Abstract

Context Patients with primary aldosteronism (PA) are at a high risk of cardiovascular diseases (CVD) and metabolic syndrome. Notable inflammatory and fibrotic changes and differential microRNA (miRNA) expression profiles in the perirenal fat observed in PA may contribute to this increased risk, however, which has not been fully elucidated.

Objective This study aimed to explore the role of high expression of miR-24-3p in perirenal fat in circulating inflammation and its correlation with a high risk of CVD in patients with PA.

Methods Perirenal fat thickness (PRFT) measured by computed tomography (CT), miR-24-3p expression in perirenal fat, circulating inflammatory factors from adrenal veins and peripheral blood in patients with PA were analyzed. In vitro, white and brown adipocytes with miR-24-3p overexpression or inhibition respectively were stimulated with aldosterone and a unidirectional co-culture model of adipocytes and HUVEC was established. The target genes of miR-24-3p were identified.

Results Patients with PA and CVD have significantly higher PRFT than those without CVD. The expression level of miR-24-3p in perirenal fat was significantly positively correlated with PRFT. MiR-24-3p was significantly upregulated in the perirenal fat of PA and was associated with increased adipogenesis, inflammation, and oxidative stress, correlating with plasma aldosterone concentration (PAC), PRFT, cardiac remodeling, and weight gain. The IL-6 level in the peripheral blood was elevated in patients with PA and CVD, and the affected adrenal vein had the highest IL-6 level. Targeting Top1, miR-24-3p modulated aldosterone-induced effects in adipocytes and influenced IL-6 secretion, thereby affecting HUVEC.

Conclusion The upregulation of miR-24-3p in the perirenal fat induced inflammation and oxidative stress by targeting Top1, which may contribute to a high risk of CVD in patients with PA.

Keywords Primary aldosteronism, Cardiovascular disease, Perirenal fat, MiR-24-3p, Inflammation, Oxidative stress

[†]Xuelin Li, Min Luo, Yanmei Zeng and Renyi Zhang contributed equally.

*Correspondence:

Meiping Guan
mpguan@163.com

Full list of author information is available at the end of the article



Introduction

Primary aldosteronism (PA), a clinical syndrome characterized by hypertension, suppressed plasma renin activity, and excess aldosterone secretion [1], stands as one of the most prevalent causes of secondary hypertension [2]. Patients with PA exhibit an elevated incidence of cardiovascular diseases (CVD) and metabolic syndrome compared to essential hypertensive counterparts [3–6]. Reversal of renin suppression after treatment is essential for improving CVD outcomes in patients with PA, but is often impeded by issues such as drug side effects. Elucidating the mechanisms underlying the high risk of CVD in patients with PA is helpful for identifying novel therapeutic targets. Previous studies have shown that high levels of aldosterone (ALD) could induce inflammation, oxidative stress and fibrosis in the heart, kidney and perirenal fat [7]. However, the link between PA-induced adipose alterations and increased risk of CVD remains unclear.

Dysfunction in visceral adipose tissue induces oxidative stress, hypoxia, and inflammation, leading to the secretion of pro-inflammatory adipokines that promote systemic inflammation and directly escalates CVD risk. Additionally, these adipokines influence metabolic processes in the liver, skeletal muscle, and heart and contribute to insulin resistance in both microvessels within adipose tissue and other vascular structures, exacerbating endothelial dysfunction and increasing CVD risk [8]. Perirenal fat, a unique visceral fat depot characterized by a distinctive composition of white and brown adipocytes [9], increases energy metabolism and the secretion of multiple adipokines and cytokines, including adiponectin (Adipoq), leptin, resistin, visfatin, TNF- α , IL-6, and IL-1 β [10].

MicroRNAs (miRNAs), non-coding RNAs consisting of 19–22 nucleotides that regulate gene expression [11], have been identified in tissues, circulation, and urine and serve as potential biomarkers and mediators in a variety of diseases [12]. Furthermore, circulating miRNAs are predominantly sourced from adipose tissue, which is broadly categorized into subcutaneous and visceral depots on the basis of morphological and locational characteristics [13]. We aimed to identify and validate the target genes of miR-24-3p, which was significantly elevated in the perirenal fat of patients with PA in this study and was previously found to be associated with aldosterone-producing adenoma (APA), CVD, and diabetes [14–17]. DNA Topoisomerase I (Top1), which is involved in DNA replication or transcription and plays a role in

regulating inflammatory mediators, has emerged as a key candidate [18–22].

This study aims to elucidate the differential miRNA expression profiles in the perirenal fat of patients with PA and their role in the high risk of CVD.

Methods

Patients and samples

The diagnostic criteria for PA were plasma aldosterone concentration (PAC) >10 ng/dL after the saline-infusion test and/or a decrease in PAC of \leq 30% after the captopril challenge test [23]. The diseases included in CVD were as previously described [24]. The study included patients aged 18–65 years old who underwent laparoscopic surgery for non-adrenal diseases (control group, n=16) or were diagnosed with PA, divided into those without CVD (PA without CVD group, n=24) and those with combined CVD (PA with CVD group, n=40). Inclusion criteria were as follows: available perirenal fat, complete clinical data, and provided informed consent. Exclusion criteria were as follows: secondary hypertension (due to conditions such as Cushing's syndrome, pheochromocytoma, renal and renovascular hypertension, hyperthyroidism, or aortic stenosis); the use of glucocorticoids, sympathomimetics, immunosuppressants, licorice, contraceptives, or medications affecting the renin–angiotensin–aldosterone system; urinary tract infections; severe malignancies; autoimmune diseases; pregnancy or breastfeeding. Unilateral laparoscopic adrenalectomy was performed for patients with PA, and perirenal fat was obtained during surgery. Venous blood was collected via adrenal venous sampling (AVS) before surgery. Perirenal fat thickness (PRFT) of patients with PA was measured as previously described [25]. The clinical characteristics of the patients were presented (Table 1). Our study was approved by the ethics committee of Southern Medical University, and written informed consent was obtained from all the patients (No: NFEC-2021-049).

Cell culture, transfection, aldosterone treatment and co-culture

Mouse 3T3-L1 preadipocytes were purchased from the type culture collection of the Chinese Academy of Sciences (Shanghai, China). Brown preadipocytes (WT-1) were a kind gift from Prof. Yu-hua Tseng's laboratory, Joslin Diabetes Center, Harvard Medical University. 3T3-L1 and WT-1 cells were cultured, differentiated, and treated with aldosterone (GlpBio, USA) following previously described methods [7]. Human umbilical

Table 1 Baseline characteristics

Characteristics	Con (n = 16)	PA without CVD (n = 24)	PA with CVD (n = 40)	p
Age (y)	53.31 ± 11.51	39.17 ± 10.07	52.30 ± 8.19	<0.001
Male, n (%)	10 (62.50)	10(41.67)	31(77.50)	0.015
Overweight/obesity, n (%)	7 (43.75)	14 (58.33)	29 (72.50)	0.447
BMI (kg/m ²)	23.50 ± 3.53	24.91 ± 3.78	25.24 ± 3.32	0.249
Systolic blood pressure (mmHg)	129 (116, 144)	140 (133, 150)	144 (130, 155)	0.027
Diastolic blood pressure (mmHg)	86 (71, 92)	92 (82, 98)	91 (81, 98)	0.270
Duration of hypertension (m)	0(0, 36)	12 (3, 24)	96 (54, 120)	<0.001
Classification of hypertension, n (%)				<0.001
0	9 (56.25)	4 (17.39)	0 (0.00)	
1	1 (6.25)	8 (34.78)	5 (12.82)	
2	3 (18.75)	6 (26.09)	11 (28.21)	
3	3 (18.75)	5 (21.74)	23 (58.97)	
Hypokalemia, n (%)	0 (0.00)	16 (76.19)	36 (94.74)	<0.001
Serum potassium (mmol/L)	4.10 (3.91, 4.26)	3.27 (2.93, 3.92)	2.97 (2.77, 3.25)	<0.001
Serum sodium (mmol/L)	141.45 ± 1.92	140.95 ± 2.09	143.03 ± 1.98	<0.001
Serum chloride (mmol/L)	107.16 ± 1.36	105.20 ± 2.16	105.14 ± 2.83	0.055
Serum calcium (mmol/L)	2.26 ± 0.07	2.29 ± 0.11	2.27 ± 0.10	0.642
Serum phosphate (mmol/L)	1.21 ± 0.17	1.15 ± 0.20	1.06 ± 0.20	0.048
BUN (mmol/L)	5.30 (4.75, 6.40)	4.20 (3.50, 5.50)	5.20 (4.60, 6.60)	0.040
Serum uric acid (μmol/L)	366.43 ± 174.72	307.00 ± 162.45	351.97 ± 136.44	0.464
Serum creatinine (μmol/L)	82.00 (68.50, 115.50)	72.00 (58.00, 94.50)	85.50 (65.00, 117.00)	0.307
eGFR (mL/min/1.73m ²)	80.04 (57.28, 105.35)	99.17 (73.62, 120.53)	85.62 (60.12, 104.07)	0.291
ALT (U/L)	22.00 (13.50,24.50)	20.00 (11.50,33.50)	20.00 (15.00,27.50)	.991
Blood glucose (mmol/L)	4.77 (4.58, 5.15)	5.04 (4.71, 5.41)	5.24 (4.83, 6.04)	0.186
Left ventricular end-diastolic diameter (mm)	42.43 ± 3.00	44.38 ± 2.90	43.33 ± 3.75	0.340
Interventricular septal thickness at end-diastole (mm)	10.00(9.00, 11.00)	10.60 (10.00, 11.60)	12.90(12.00, 13.00)	<0.001
Left ventricular posterior wall thickness at end-diastole (mm)	9.39 ± 1.52	10.15 ± 0.93	12.18 ± 0.98	<0.001
Left ventricular end-diastolic volume (mL)	83.00 (76.00, 92.50)	83.00 (74.00, 92.00)	83.00 (70.00, 102.00)	0.944
Left ventricular end-systolic volume (mL)	27.00 (24.50, 33.50)	30.00 (27.00, 32.00)	30.00 (25.00, 35.00)	0.535
Fractional shortening (%)	36.00 (35.00, 37.00)	34.00 (33.00, 37.00)	35.00 (32.00, 36.00)	0.306
Ejection fraction (%)	66.00 (65.00, 67.00)	64.00 (62.00, 67.00)	64.00 (61.00, 66.50)	0.191
Stroke volume (mL)	53.00 (50.00, 59.00)	55.00 (49.00, 63.00)	50.00 (45.00, 64.50)	0.607
Aortic sclerosis, n (%)	9 (56.25%)	5 (20.83%)	30 (75.00%)	<0.001
Aldosterone (ng/dL)	–	25.57 (19.15, 39.50)	38.71 (25.33, 62.45)	0.290
Plasma renin activity (ng/mL/h)	–	0.32 (0.10, 0.48)	0.17 (0.10, 0.38)	0.336
ARR	–	96.38 (67.67, 255.70)	236.70 (78.06, 433.00)	0.124

Bold value indicates that the difference is statistically significant ($p < 0.05$)

vein endothelial cells (HUVEC) were cultured in high-glucose DMEM (Gibco, USA) supplemented with 10% fetal bovine serum in a 37 °C incubator with 5% CO₂. For transfection, the cells were transfected with the miR-24-3p mimic or inhibitor (Ribobio, Guangzhou, China), Top1 overexpression plasmid (Miaoling, Wuhan, China), or luciferase reporter plasmid using jetPRIME transfection reagent (Polyplus, France). For co-culture, after adipocyte intervention, the medium was replaced with fresh serum-free medium, and the

cells were cultured for 48 h. The supernatant was then collected, centrifuged at 260×g for 10 min, and added to HUVEC, which were collected and assayed after 24 h of stimulation.

RNA extraction, reverse transcription, and quantitative PCR (qPCR)

Total RNA was extracted from perirenal fat or cells utilizing TRIzol reagent (Vazyme, Nanjing, China). Reverse transcription was executed using 500 ng of total

RNA with the Evo M-MLV RT Master Mix (AG11706, Guangzhou, China) following the manufacturer's guidelines. For miRNA, reverse transcription was performed with a miRNA cDNA First Strand Synthesis Kit (by tailing A, AG11716, Guangzhou, China) and an Evo M-MLV RT Kit for qPCR (by stem-loop, AG11707, Guangzhou, China). QPCR was performed using Cham Q Universal SYBR qPCR Master Mix (Vazyme, Nanjing, China) and an ABI QuantStudio 5 Real-Time PCR system (Applied Biosystems, USA). The thermal cycling conditions were as follows: initial denaturation at 95 °C for 30 s; 40 cycles at 60 °C for 35 s; and a final extension at 60 °C for 34 s. The mRNA and miRNA expression levels were quantified using the $2^{-\Delta\Delta CT}$ method and normalized to 18S/ β -ACTIN and U6, respectively. Primer sequences for qPCR are provided in the Supplementary material (Table S1).

Western blotting analysis

Cells and perirenal fat were lysed using RIPA lysis buffer containing PMSF and phosphatase inhibitor, followed by centrifugation at 13,000 rpm for 30 min at 4 °C. Equal amounts of protein were separated by SDS-PAGE and then transferred onto a PVDF membrane. The membrane was blocked with 5% BSA for 1 h and then incubated with the primary antibody at 4 °C overnight. After being washed for five times with TBST, the membrane was incubated for 1 h at room temperature with an HRP-conjugated secondary antibody. The signal was detected using the BLT Pro chemiluminescence detection system (BLT, Guangzhou, China), and the band intensity was quantified via ImageJ software. α -Tubulin or β -ACTIN served as the internal reference control. Detailed information on the antibodies used is provided in the Supplementary material (Table S2).

Enzyme linked immunosorbent assay (ELISA)

The levels of IL-6 in human serum and adipocyte supernatants were measured using ELISA kits. Human IL-6 and mouse IL-6 were quantified with kits from CloudClone (Wuhan, China) and FineTest (Wuhan, China) respectively. All procedures were carried out according to the manufacturer's instructions.

Measurement of reduced glutathione (GSH) levels

The serum GSH concentration was determined using a GSH assay kit from Nanjing Jiancheng (Nanjing, China). Reagents were added according to the operation, and the OD value of each well was read at 405 nm using a microplate reader.

Reactive oxygen species (ROS) assay

Cellular ROS activities were assessed with a ROS assay kit from Beyotime (Shanghai, China) following the manufacturer's protocol. The detection was performed using either an inverted fluorescence microscope (Nikon, Japan) or a SpectraMax i3x microplate reader (Molecular Devices, USA).

Oil red O staining

Cells were fixed in 10% neutral formaldehyde solution for 30 min, permeabilized with 60% isopropanol for 10 s, and stained with Oil Red O at room temperature for 30 min. Cells were subsequently washed with 60% isopropanol for 10 s, rinsed with PBS, and imaged using a Motorized inverted microscope IX73 (Olympus, Japan).

Dual-luciferase reporter assay

Luciferase reporter plasmids were designed by Kidanbio (Guangzhou, China). WT-1 were transfected with the miR-24-3p mimic (or mimic NC) and related reporter plasmids in 96-well plates. After 24–48 h of transfection, the luciferase activity was analyzed using luciferase assay kits (Yeasen, Wuhan, China) according to the manufacturer's instructions.

Statistical analyses

All the statistical analyses were conducted via SPSS version 23.0 software. Normally distributed variables are presented as mean \pm standard deviation (SD), while non-normally distributed variables are presented as median and interquartile range (IQR). Categorical variables are expressed as frequencies (percentages). Comparisons between two normally distributed continuous variables were made via Student's t test, whereas comparisons between non-normally distributed variables were carried out via Mann–Whitney U test. For clinical indicators involving three groups, one-way analysis of variance (ANOVA) was applied for normally distributed data, and the Kruskal–Wallis test was used for non-normally distributed data. Categorical variables were compared using the chi-square test. Relationships between normally distributed continuous variables were analyzed via Pearson's correlation coefficient, whereas Spearman's rank correlation was used for non-normally distributed continuous variables. A p value < 0.05 was considered statistically significant.

Results

Patient characteristics

This study included 64 patients with PA and 16 patients in the control group. The PA group was divided into the PA without CVD group (n=24) and the PA with CVD group (n=40). Clinical data were collected and analyzed

(Table 1). Age differences were significant across groups, with mean ages of 53.31 years for the control group, 39.17 years for the PA without CVD group, and 52.30 years for the PA with CVD group. Sex distribution varied, with 62.5% males in the control group, 41.67% in the PA without CVD group, and 77.5% in the PA with CVD group. The PA with CVD group presented the longest hypertension duration (median of 96 months), highest hypertension severity (58.97% with Grade 3), most severe hypokalemia (94.74%), highest prevalence of aortic atherosclerosis (75%), lowest serum potassium and phosphorus levels, and highest serum sodium levels. Cardiac ultrasound revealed increasing septal and left ventricular posterior wall end-diastolic thicknesses across the three groups ($p < 0.001$), with septal thicknesses of 10.00 mm, 10.60 mm, and 12.90 mm, and posterior wall thicknesses of 9.39 mm, 10.15 mm, and 12.18 mm, respectively.

Expression of miR-24-3p and its clinical correlations in patients with PA

Among the miRNAs reported to be differentially expressed in patients with PA (miR-203, miR-7-5p, miR-193, miR-30e-5p, miR-24-3p, miR-299, and miR-223), miR-24-3p was significantly upregulated in the perirenal fat of patients with PA ($n = 5$) compared with the control group ($n = 5$) (Fig. 1A). Further analysis with a larger sample size, including a control group ($n = 16$), a PA without CVD group ($n = 24$), and a PA with CVD group ($n = 40$), confirmed significantly higher miR-24-3p expression in patients with PA, with greater upregulation in the PA with CVD group (Fig. 1B).

Correlation analysis revealed that miR-24-3p expression in the perirenal fat of patients with PA was positively correlated with PAC ($r = 0.3173$, $p = 0.0162$), left ventricular posterior wall end-diastolic thickness ($r = 0.2862$, $p = 0.0378$), and BMI ($r = 0.2910$, $p = 0.0218$) and negatively correlated with PaO₂ ($r = -0.3984$, $p = 0.0146$) (Fig. 1C–F). The PRFT was measured by abdominal computed tomography (CT) in patients with PA as shown (Fig. 1G). Since surgeons typically remove the culprit adrenal gland, perirenal fat was collected from the affected side only. MiR-24-3p expression in

perirenal fat was significantly positively correlated with the PRFT on the affected side ($r = 0.4903$, $p = 0.0001$), the intact side (contralateral to the affected side, $r = 0.4332$, $p = 0.0009$), and the total (the sum of both sides, $r = 0.4689$, $p = 0.0003$) (Fig. 1H–J). Compared with the PA without CVD group, the PA with CVD group had significantly greater PRFT on the affected side, the intact side, and the total (Fig. 1K–M).

Patients with PA were classified into high and low miR-24-3p expression groups on the basis of median miR-24-3p levels. The high miR-24-3p group had higher PAC, BMI, overweight/obesity proportion, hypertension duration, interventricular septum and left ventricular posterior wall end-diastolic thickness, PaCO₂, HCO₃⁻, and extracellular residual bases, also lower PaO₂ and serum phosphorus levels than the low miR-24-3p group (Table 2).

Adipogenesis, inflammation and oxidative stress in perirenal fat and serum characterization in patients with PA

The expression of adipogenic genes such as CCAAT enhancer binding protein alpha (C/EBP α), PPARG coactivator 1 alpha (PGC1 α), and uncoupling protein 1 (UCP1) were elevated in the perirenal fat of patients with PA. Additionally, genes related to oxidative stress, such as nuclear factor erythroid 2-related factor 2 (NRF2), heme oxygenase 1 (HO-1), NADPH oxidase 4 (NOX4), and inflammation (IL-6), were significantly increased (Fig. 2A). Protein level analysis confirmed that adipogenesis, inflammation, and oxidative stress were significantly upregulated in the perirenal fat of patients with PA, consistent with the changes in transcript levels (Fig. 2B). Moreover, oxidative stress levels were greater in the perirenal fat of the PA with CVD group than in that of the PA without CVD group (Fig. 2C).

Serum IL-6 and GSH levels in patients with PA were measured at various sites of AVS. For those diagnosed with unilateral APA, IL-6 levels were significantly higher and GSH levels were lower in the affected adrenal vein than in both the intact adrenal vein

(See figure on next page.)

Fig. 1 MiR-24-3p expression and its clinical correlations in patients with PA. **A** Screening of differential miRNAs in the perirenal fat of controls and patients with PA. **B** Relative miR-24-3p expression in perirenal fat in the control group, PA with CVD group and PA without CVD group. **C–F** Correlations between miR-24-3p expression and PAC (**C**), left ventricular posterior wall end-diastolic thickness (**D**), BMI (**E**), and PaO₂ (**F**). **G** Measurement patterns of the PRFT in abdominal CT. **H–J** Correlations between miR-24-3p expression and PRFT on the affected side (**H**), the intact side (**I**), and the total (**J**). **K–M** Differences in PRFT between the PA without CVD group and the PA with CVD group on the affected side (**K**), the intact side (**L**), and the total (**M**). Dividing lines indicate the splicing of lanes from the same gel to remove irrelevant lanes. * $p < 0.05$, ** $p < 0.01$, *** $p < 0.001$, $n \geq 3$

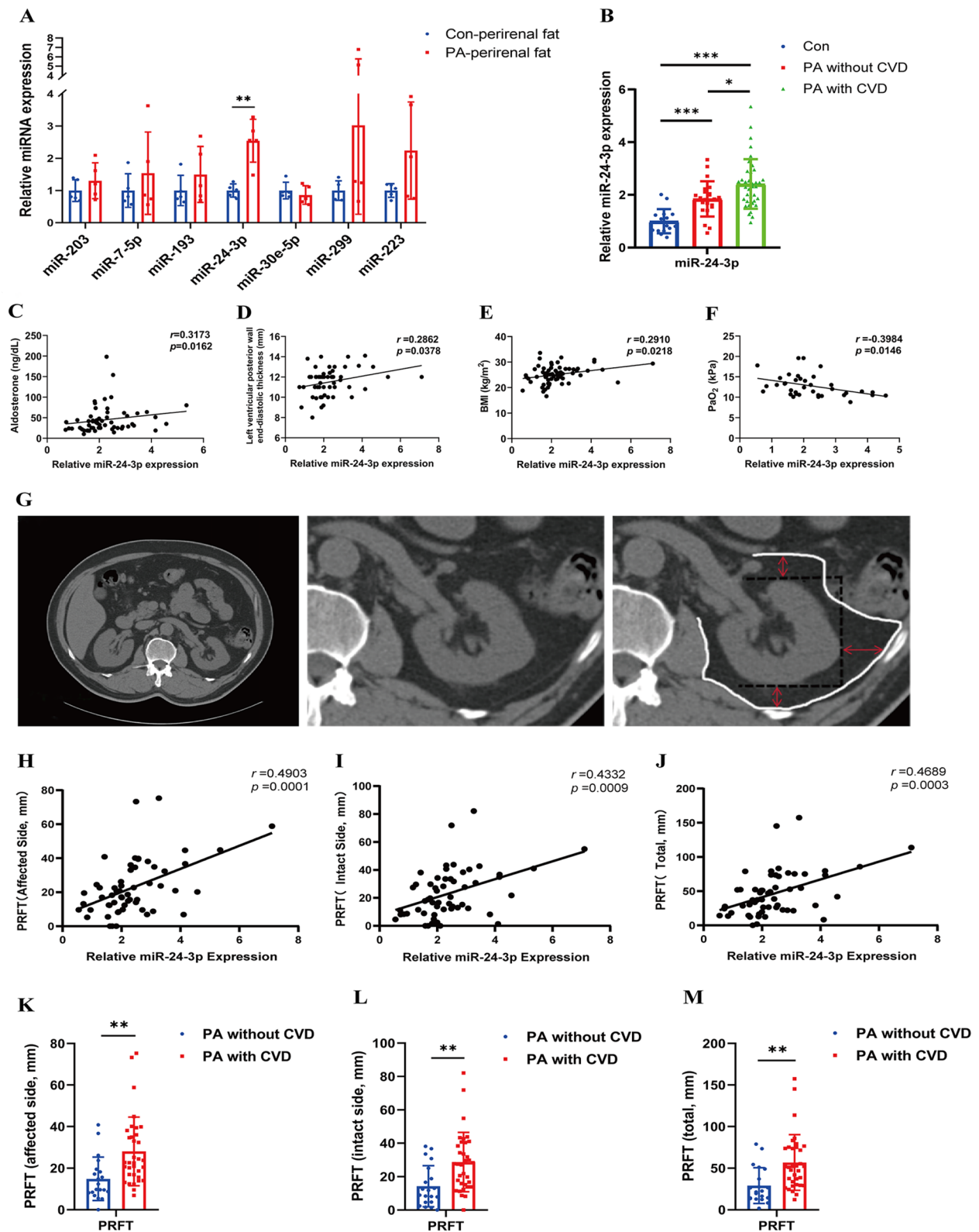


Fig. 1 (See legend on previous page.)

Table 2 Comparisons of clinical characteristics between the high and low miR-24-3p groups

Characteristics	Low miR-24-3p (n = 32)	High miR-24-3p (n = 32)	p
Age (y)	46.50 ± 10.67	48.25 ± 11.29	0.526
Male, n (%)	13 (40.63)	10 (31.25)	0.602
Overweight/obesity, n (%)	18 (56.25%)	27 (84.38%)	0.027
BMI (kg/m ²)	24.22 ± 3.93	26.08 ± 2.63	0.032
Systolic blood pressure (mmHg)	144 (132, 157)	142 (130, 152)	0.672
Diastolic blood pressure (mmHg)	94 (81, 101)	91 (81, 96)	0.359
Duration of hypertension (m)	24 (5, 96)	84 (5, 120)	0.013
Serum potassium (mmol/L)	3.12 (2.81, 3.61)	2.98 (2.77, 3.58)	0.720
Serum sodium (mmol/L)	142.16 ± 2.27	142.48 ± 2.23	0.591
Serum chloride (mmol/L)	105.15 ± 2.43	105.18 ± 2.82	0.966
Serum calcium (mmol/L)	2.28 ± 0.10	2.27 ± 0.10	0.649
Serum phosphate (mmol/L)	1.14 ± 0.19	1.02 ± 0.20	0.027
BUN (mmol/L)	4.90 (4.00, 7.20)	4.80 (4.30, 5.50)	0.736
Serum uric acid (μmol/L)	321.03 ± 122.38	354.19 ± 170.02	0.393
Serum creatinine (μmol/L)	74.00 (61.50, 97.50)	91.00 (70.00, 109.00)	0.138
Cys-C (mg/L)	0.87 (0.79, 1.11)	0.96 (0.89, 1.10)	0.213
eGFR (mL/min/1.73m ²)	98.32 (68.82, 109.12)	85.23 (64.63, 100.23)	0.203
ALT (U/L)	18.00 (11.50, 23.00)	21.00 (16.50, 32.50)	0.072
TG (mmol/L)	1.30 (0.90, 1.57)	1.60 (0.99, 2.67)	0.170
CHOL (mmol/L)	4.23 (3.86, 5.55)	4.33 (3.59, 5.28)	0.605
HDL-C (mmol/L)	1.08 ± 0.22	1.04 ± 0.20	0.457
LDL-C (mmol/L)	2.67 (2.42, 3.38)	2.64 (2.25, 3.44)	0.553
Blood glucose (mmol/L)	4.98 (4.63, 5.41)	5.33 (4.85, 6.06)	0.213
pH	7.42 ± 0.03	7.43 ± 0.03	0.597
PaCO ₂ (kPa)	5.28 ± 0.51	5.65 ± 0.48	0.027
PaO ₂ (kPa)	13.15 (11.30, 14.95)	11.20 (10.50, 13.00)	0.023
HCO ₃ ⁻ (mmol/L)	25.27 ± 2.80	27.39 ± 2.23	0.017
Extracellular residual bases (mmol/L)	1.25 ± 2.80	3.26 ± 2.23	0.023
Left ventricular end-diastolic diameter (mm)	43.08 ± 3.26	44.35 ± 3.70	0.207
Interventricular septal thickness at end-diastole (mm)	12.00 (10.50, 12.85)	12.50 (12.00, 13.00)	0.026
Left ventricular posterior wall thickness at end-diastole (mm)	11.17 ± 1.45	11.90 ± 1.17	0.049
Left ventricular end-diastolic volume (mL)	79.00 (72.00, 90.00)	87.50 (74.00, 102.00)	0.437
Left ventricular end-systolic volume (mL)	27.00 (25.00, 33.50)	32.00 (25.00, 38.00)	0.420
Fractional shortening (%)	34.00 (33.00, 35.50)	35.00 (31.00, 38.00)	0.694
Ejection fraction (%)	64.00 (62.00, 65.00)	64.50 (59.00, 68.00)	0.810
Aldosterone (ng/dL)	31.74 (20.70, 43.20)	38.71 (26.38, 68.50)	0.038
Plasma renin activity (ng/mL/h)	0.24 (0.10, 0.50)	0.17 (0.10, 0.33)	0.898
ARR	130.50 (61.39, 312.53)	191.50 (89.63, 426.51)	0.371

Bold value indicates that the difference is statistically significant ($p < 0.05$)

and peripheral blood, with no significant differences between the intact adrenal vein and peripheral blood for either marker (Fig. 2D, E). Additionally, IL-6 levels in the peripheral blood were significantly greater in the PA with CVD group than in the PA without CVD group (Fig. 2F).

Effects of miR-24-3p and aldosterone on adipocytes

During the differentiation of 3T3-L1 and WT-1, miR-24-3p expression increased over time and was significantly higher at the end of differentiation than at D0 (Fig. 3A, B). In 3T3-L1 overexpressing miR-24-3p throughout differentiation, Oil Red O staining at D8 revealed a significant increase in lipid droplets, whereas cells with miR-24-3p inhibition showed a significant reduction in lipid droplets (Fig. 3C).

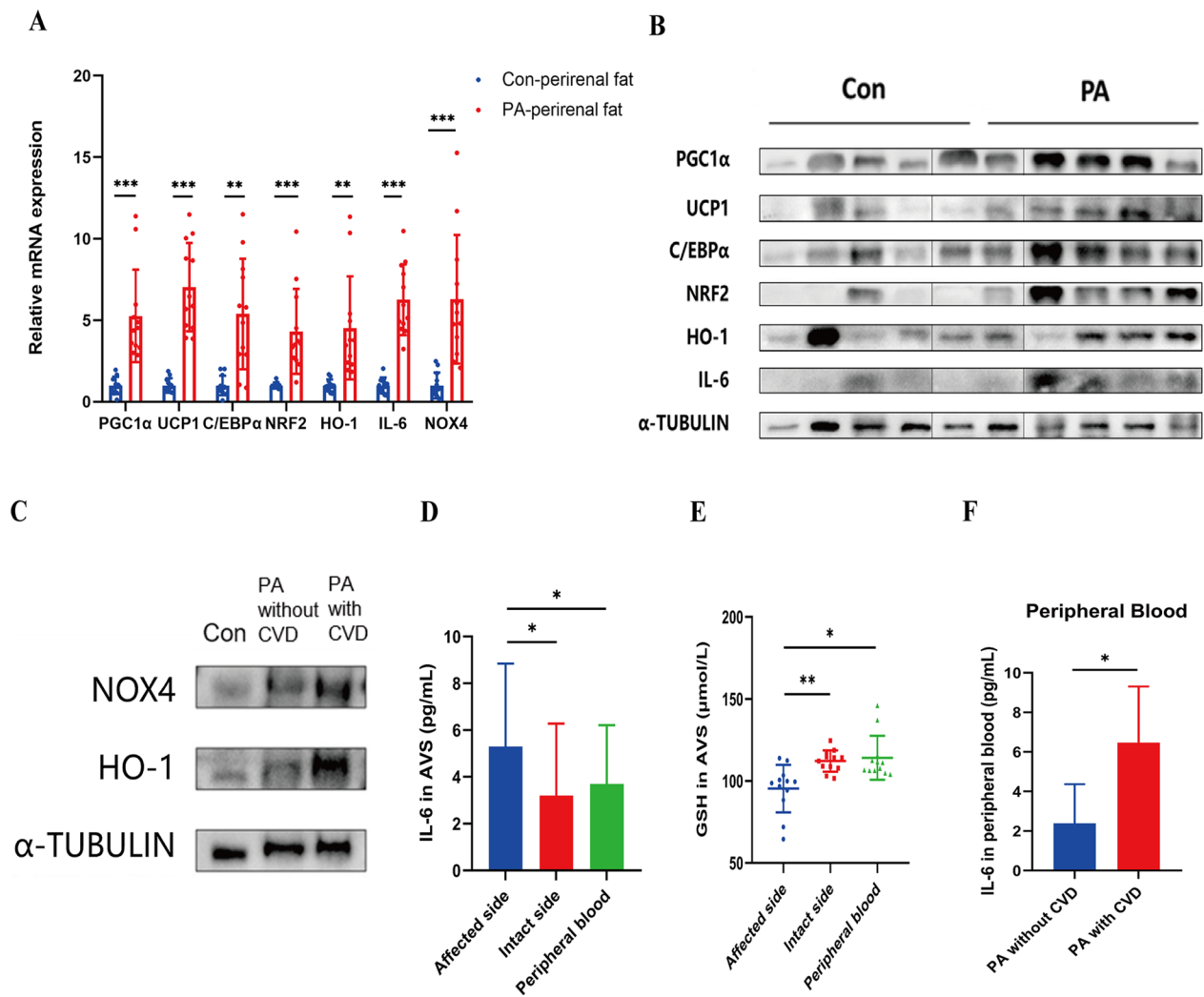


Fig. 2 Perirenal fat and serum characterization in patients with PA. **A, B** Differences in adipogenesis, inflammation, and oxidative stress markers in perirenal fat between controls and patients with PA at the transcript levels (**A**) and protein levels (**B**). **C** Protein levels of oxidative stress markers in the perirenal fat of the control group, the PA with CVD group, and the PA without CVD group. **D, E** IL-6 (**D**) and GSH (**E**) levels in affected and intact adrenal veins and peripheral blood in patients with PA. **F** IL-6 levels in the peripheral blood of the PA with CVD group compared with the PA without CVD group. * $p < 0.05$, ** $p < 0.01$, *** $p < 0.001$, $n \geq 3$

MiR-24-3p expression and the adipocyte phenotype were investigated at various time points of aldosterone stimulation. Continuous aldosterone stimulation from

the preadipocyte stage of 3T3-L1 and WT-1 markedly upregulated miR-24-3p expression in both cell types after differentiation into adipocytes (Fig. 3D, E). Additionally,

(See figure on next page.)

Fig. 3 MiR-24-3p expression and effects of aldosterone stimulation on adipocytes. **A, B** Expression of miR-24-3p during the differentiation of 3T3-L1 (**A**) and WT-1 (**B**). **C** Changes in adipogenesis following miR-24-3p overexpression or inhibition throughout 3T3-L1 differentiation. Oil Red O staining showed lipid droplets. **D–G** Changes in miR-24-3p expression with continuous aldosterone stimulation from the preadipocyte stage of 3T3-L1 (**D**) and WT-1 (**E**) to mature adipocytes; changes in miR-24-3p expression with aldosterone stimulation applied after maturation in white adipocytes (**F**) and brown adipocytes (**G**). **H–K. H** Changes in adipocyte phenotypes with continuous aldosterone stimulation from the preadipocyte stage of 3T3-L1 to mature white adipocytes; **I** changes in adipocyte phenotypes with aldosterone stimulation applied after maturation in white adipocytes; **J** changes in adipocyte phenotypes with continuous aldosterone stimulation from the preadipocyte stage of WT-1 to mature brown adipocytes; **K** changes in adipocyte phenotypes with aldosterone stimulation applied after maturation in brown adipocytes. (**A, B**: vs D0), * $p < 0.05$, ** $p < 0.01$, *** $p < 0.001$, $n \geq 3$

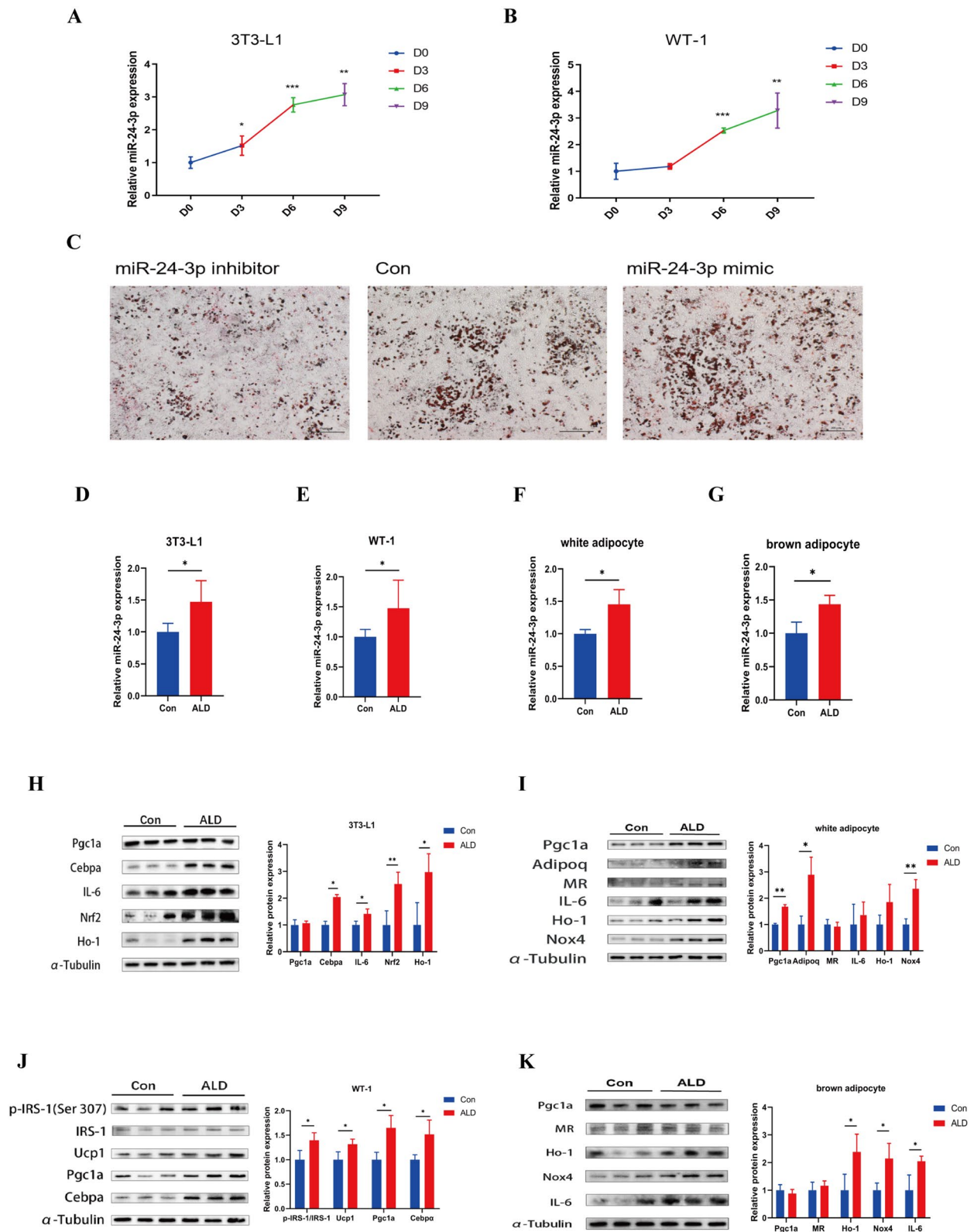


Fig. 3 (See legend on previous page.)

aldosterone stimulation applied after maturation significantly increased miR-24-3p expression in both white and brown adipocytes (Fig. 3E, G).

Furthermore, during continuous exposure of 3T3-L1 to aldosterone starting at D0, we observed notable elevations in the protein levels of the adipogenesis marker (Cebp α), and the inflammatory and oxidative stress markers (IL-6, Nrf2, Ho-1) in the aldosterone group, with no significant changes in Pgc1 α (Fig. 3H). Treating mature white adipocytes with aldosterone significantly elevated protein levels associated with adipogenesis and oxidative stress (Fig. 3I). In addition, continuous aldosterone stimulation throughout WT-1 differentiation and applied merely after maturation both resulted in increased adipogenesis, inflammation, and oxidative stress (Fig. 3J, K).

Comprehensive effects of miR-24-3p and aldosterone on adipocytes and subsequent impact on HUVEC

In white adipocytes, miR-24-3p overexpression significantly increased adipogenesis, whereas its inhibition substantially reduced adipogenesis and inflammation (Fig. 4A). MiR-24-3p played a similar role in brown adipocytes (Fig. 4B).

White adipocytes were treated with aldosterone and the miR-24-3p inhibitor (or inhibitor NC). Consistent with previous results, adipogenesis, oxidative stress and insulin resistance were greater in the aldosterone+inhibitor NC group than in the control group, while miR-24-3p inhibition tended to ameliorate these phenotypes (Fig. 4C). Similar treatment in brown adipocytes showed that aldosterone increased adipogenesis and oxidative stress, whereas miR-24-3p inhibition mitigated these phenotypes to some degree (Fig. 4D).

ROS levels were detected in the aforementioned subgroups of white adipocytes. MiR-24-3p inhibition significantly reduced aldosterone-mediated increase in ROS levels (Fig. 4E). The results of the quantitative ROS staining experiments with a microplate reader were similar to those of the qualitative experiments (Fig. 4F). Brown adipocytes subjected to the same treatment exhibited similar results (Fig. 4E, G).

Furthermore, we established a unidirectional co-culture model of HUVEC and adipocytes under aldosterone and

miR-24-3p intervention (Supplementary material, Figure S1). HUVEC cultured in conditioned medium (CM) from white adipocytes treated with aldosterone and inhibitor NC showed significant upregulation of the intercellular adhesion molecule ICAM1 and angiogenic factor VEGFA transcript expressions, along with increased expression of inflammatory markers (PTGS2, TNF- α , and IL-6). The transcript levels of senescence markers (P53 and P21) and an apoptosis marker (BAX) were also significantly increased. These phenotypes were markedly ameliorated in HUVEC cultured in CM from white adipocytes treated with aldosterone and the miR-24-3p inhibitor (Fig. 4H).

In HUVEC cultured with CM from brown adipocytes treated with aldosterone and inhibitor NC, adhesion, inflammation, oxidative stress, and senescence were exacerbated. In comparison, CM from brown adipocytes treated with aldosterone and the miR-24-3p inhibitor significantly downregulated PTGS2 and HO-1, whereas other markers tended to decrease without statistical significance (Fig. 4I).

Identification and validation of Top1 as a target gene of miR-24-3p

The ENCORI database was used to identify common miR-24-3p target genes in human and murine sources (Fig. 5A). This analysis revealed 88 genes, from which we focused on 10 genes (Rbp4, Kat6a, Fzd5, Ctnnb1, Top1, Rala, Sp1, Rap1b, Rab4b, and Pak4) on the basis of the literature and gene annotations. The transcript levels of these genes were examined in miR-24-3p-intervened adipocytes and the perirenal fat from patients with PA. In brown adipocytes transfected with the miR-24-3p mimic, Kat6a, Fzd5, Top1, and Pak4 expressions were downregulated (Fig. 5B). In white adipocytes treated with aldosterone and the miR-24-3p mimic, Kat6a, Ctnnb1, Top1, Rala, and Rab4b levels were decreased (Fig. 5C). In white adipocytes exposed to aldosterone and the miR-24-3p inhibitor, Kat6a, Fzd5, Top1, and Pak4 were elevated (Fig. 5D). In the perirenal fat of patients with PA, the TOP1 and PAK4 transcript levels were significantly reduced (Fig. 5E). Since transcript level changes across all four models were consistent with the regulatory role of miR-24-3p, we focused subsequent investigations on Top1.

(See figure on next page.)

Fig. 4 Comprehensive effects of miR-24-3p and aldosterone on adipocytes and their subsequent impact on HUVEC. **A, B** Effects of miR-24-3p intervention on white (**A**) and brown adipocytes (**B**). **C, D** Effects of miR-24-3p inhibition on aldosterone-induced white (**C**) and brown adipocyte phenotypes (**D**). **E** ROS staining in white and brown adipocytes treated with aldosterone and inhibited by miR-24-3p. **F, G** Quantitative ROS levels in white (**F**) and brown adipocytes (**G**) treated with aldosterone and inhibited by miR-24-3p. **H, I** Effects of aldosterone and the miR-24-3p inhibitor in CM from white (**H**) and brown adipocytes (**I**) on HUVEC. * $p < 0.05$, ** $p < 0.01$, *** $p < 0.001$, $n \geq 3$

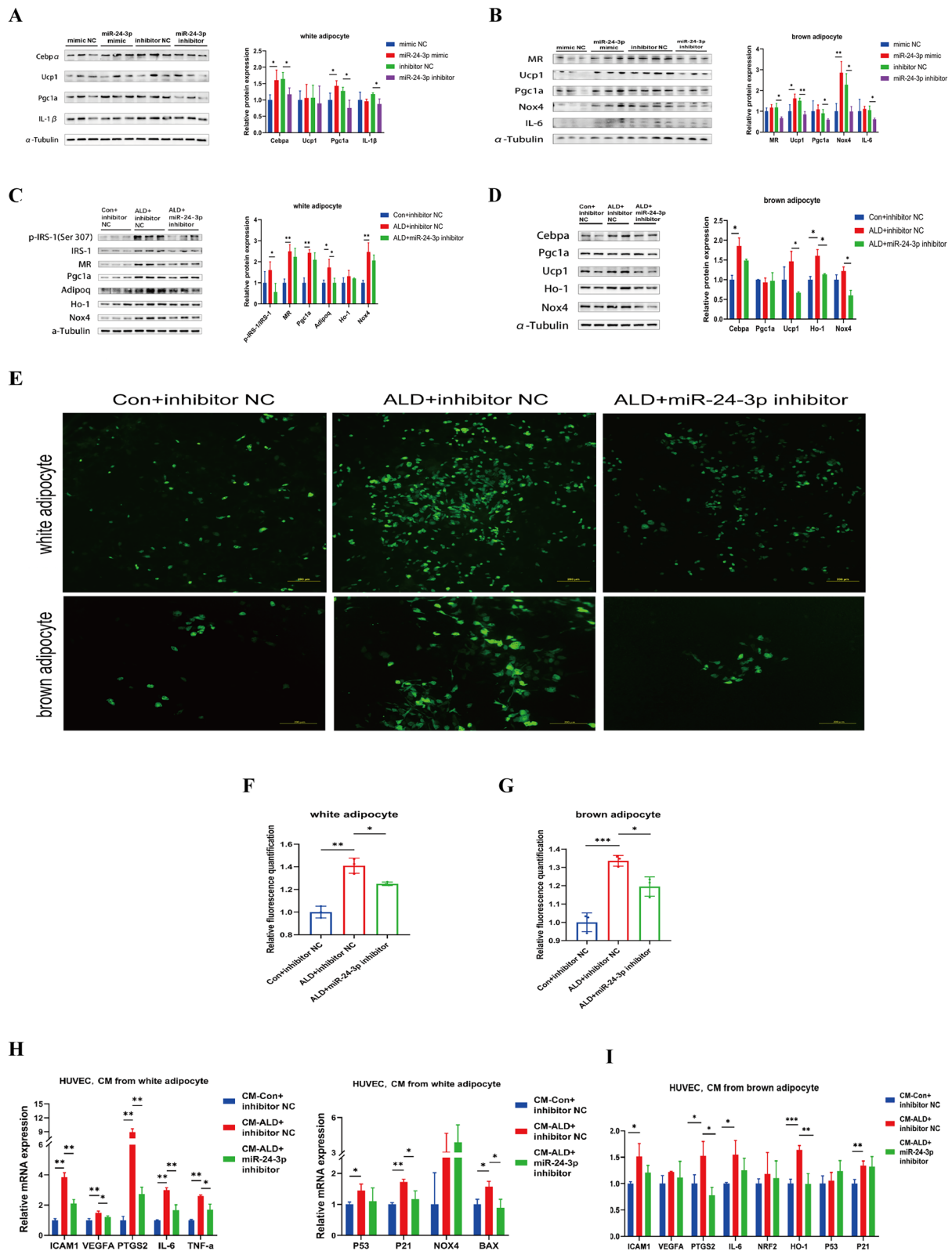


Fig. 4 (See legend on previous page.)

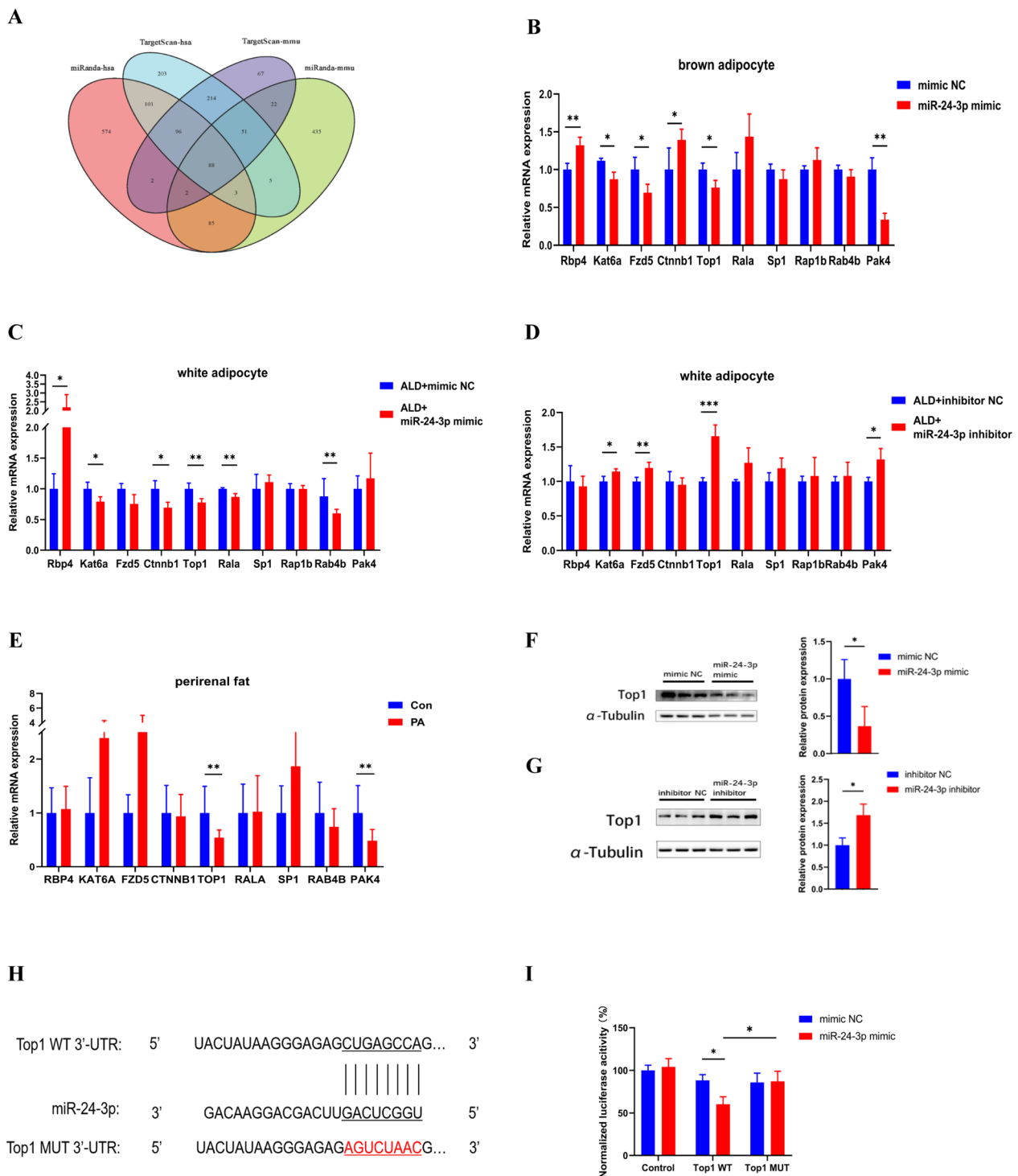


Fig. 5 Identification and validation of Top1 as a target gene of miR-24-3p. **A** Venn diagram of common target genes of miR-24-3p in humans and mice according to TargetScan and miRanda. **B** The transcript levels of target genes in brown adipocytes transfected with the miR-24-3p mimic. **C** The transcript levels of target genes in white adipocytes treated with aldosterone and the miR-24-3p mimic. **D** The transcript levels of target genes in white adipocytes exposed to aldosterone and the miR-24-3p inhibitor. **E** The transcript levels of target genes in the perirenal fat of patients with PA. **F, G** The protein levels of Top1 after transfection of the miR-24-3p mimic (**F**) or the miR-24-3p inhibitor (**G**) into adipocytes. **H** Sequences of the Top1 3' UTR containing the miR-24-3p binding sites and the constructed mutant sequences. **I** Determination of luciferase activity after co-transfection with the miR-24-3p mimic and reporter plasmids in 3T3-L1. * $p < 0.05$, ** $p < 0.01$, *** $p < 0.001$, $n \geq 3$

The protein level of Top1 was significantly downregulated after the transfection of the miR-24-3p mimic into adipocytes (Fig. 5F), whereas the miR-24-3p inhibitor markedly upregulated the Top1 protein level (Fig. 5G). WT-1 were co-transfected with a dual-luciferase vector containing the wild-type Top1 3'-UTR target site and the miR-24-3p mimic (Fig. 5H). Co-transfection of the miR-24-3p mimic and the wild-type Top1 3'-UTR vector decreased luciferase activity by approximately 40%, whereas mutation of the miR-24-3p seed region within the Top1 3'-UTR abrogated the repressive effect of the miRNA (Fig. 5I). Thus, miR-24-3p directly binds the 3'-UTR of Top1 and plays an inhibitory role, confirming Top1 as a target of miR-24-3p.

Effects of miR-24-3p and Top1 modulation on adipocytes and subsequent impact on HUVEC

Adipocytes were co-transfected with the miR-24-3p mimic and Top1 overexpression plasmid (and their controls mimic NC and Top1 NC). Compared with the aldosterone+mimic NC+Top1 NC group, the protein levels of Ucp1, IL-6, Ho-1, and Nox4 were significantly upregulated in the aldosterone+mimic+Top1 NC group, whereas these levels were downregulated in the aldosterone+mimic+Top1 group (Fig. 6A). ROS staining revealed a significantly higher proportion of staining-positive cells under a fluorescence microscope in the aldosterone+mimic+Top1 NC group compared with the aldosterone+mimic NC+Top1 NC group. In contrast, the aldosterone+mimic+Top1 group had a notably lower proportion of ROS-positive cells than the aldosterone+mimic+Top1 NC group (Fig. 6B). Quantitative analysis via a microplate reader revealed that the fluorescence intensity in the aldosterone+mimic+Top1 group was significantly lower than that in the aldosterone+mimic+Top1 NC group (Fig. 6C).

The Top1 inhibitor Camptothecin (CPT) significantly upregulated the transcript levels of inflammatory markers (IL-6 and TNF- α), oxidative stress markers (Nox4, Nrf2, and Ho-1), and an apoptosis marker (Bax) in adipocytes (Fig. 6D), as well as the protein levels of IL-6 and Nox4 (Fig. 6E). Furthermore, IL-6 levels in

the adipocyte supernatant were significantly increased after Top1 inhibition (Fig. 6F). CM from Top1-inhibited adipocytes was used in a unidirectional co-culture with HUVEC, resulting in significantly elevated transcript levels of enhanced adhesion (ICAM1), inflammation (PTGS2, IL-6, and TNF- α), and oxidative stress (HO-1 and Nox4), as well as protein levels of PTGS2, IL-6, and HO-1 (Fig. 6G, H).

Discussion

In this study, we identified increased miR-24-3p expression, inflammation and oxidative stress in perirenal fat in patients with PA. The significant difference in both IL-6 and GSH levels between the affected adrenal vein and peripheral blood in patients with unilateral APA indicates that perirenal fat may be the origin of circulating inflammation, thereby exacerbating endothelial damage. This is closely associated with the elevated CVD risk in patients with PA. The overall mechanism of the findings is illustrated in Fig. 7.

Previous studies have shown that miR-24-3p targets CYP11B2 in APA, affecting aldosterone synthesis [14]. In a myocardial ischemic mouse model, miR-24 expression is upregulated in endothelial cells, targeting GATA2 and PAK4 to induce apoptosis [15]. Circulating miR-24 levels are reduced in patients with type 2 diabetes mellitus [16], while miR-24 expression in subcutaneous fat is elevated in patients with HIV [17]. We observed elevated miR-24-3p expression in the perirenal fat of patients with PA, correlating with an increased CVD risk, which prompted an investigation of miR-24-3p in adipocytes. Two previous studies have demonstrated changes in miR-24 expression during 3T3-L1 differentiation [26, 27]. Jin et al. reported significant upregulation of miR-24 during 3T3-L1 differentiation, with overexpression inhibiting MAPK7 and promoting adipogenesis [27]. Our results show that miR-24-3p expression gradually increases during differentiation of 3T3-L1 or WT-1. The overexpression of miR-24-3p significantly promotes adipogenesis. This may explain the positive correlation between miR-24-3p expression and BMI, as well as between miR-24-3p expression and PRFT, suggesting that dysregulation of miR-24-3p in perirenal fat is closely

(See figure on next page.)

Fig. 6 Effects of miR-24-3p and Top1 modulation on adipocytes and subsequent impact on HUVEC. **A** Effects of co-transfection of the miR-24-3p mimic with the Top1 overexpression plasmid on aldosterone-stimulated adipocytes at the protein levels. **B** ROS staining in adipocytes treated with aldosterone, the miR-24-3p mimic, and the Top1 overexpression plasmid. **C** Quantitative ROS levels in adipocytes treated with aldosterone, the miR-24-3p mimic, and the Top1 overexpression plasmid. **D** Effects of Top1 inhibition on adipocytes at the transcript levels. **E** Effects of Top1 inhibition on adipocytes at the protein levels. **F** IL-6 levels in supernatants of adipocytes with Top1 inhibition. **G, H** Effects of Top1 inhibition in adipocytes on HUVEC at the transcript levels (**G**) and protein levels (**H**). M-NC: mimic NC; mimic: miR-24-3p mimic; T-NC: pCMV-Top1-NC; Top1: pCMV-Top1. * $p < 0.05$, ** $p < 0.01$, *** $p < 0.001$, $n \geq 3$

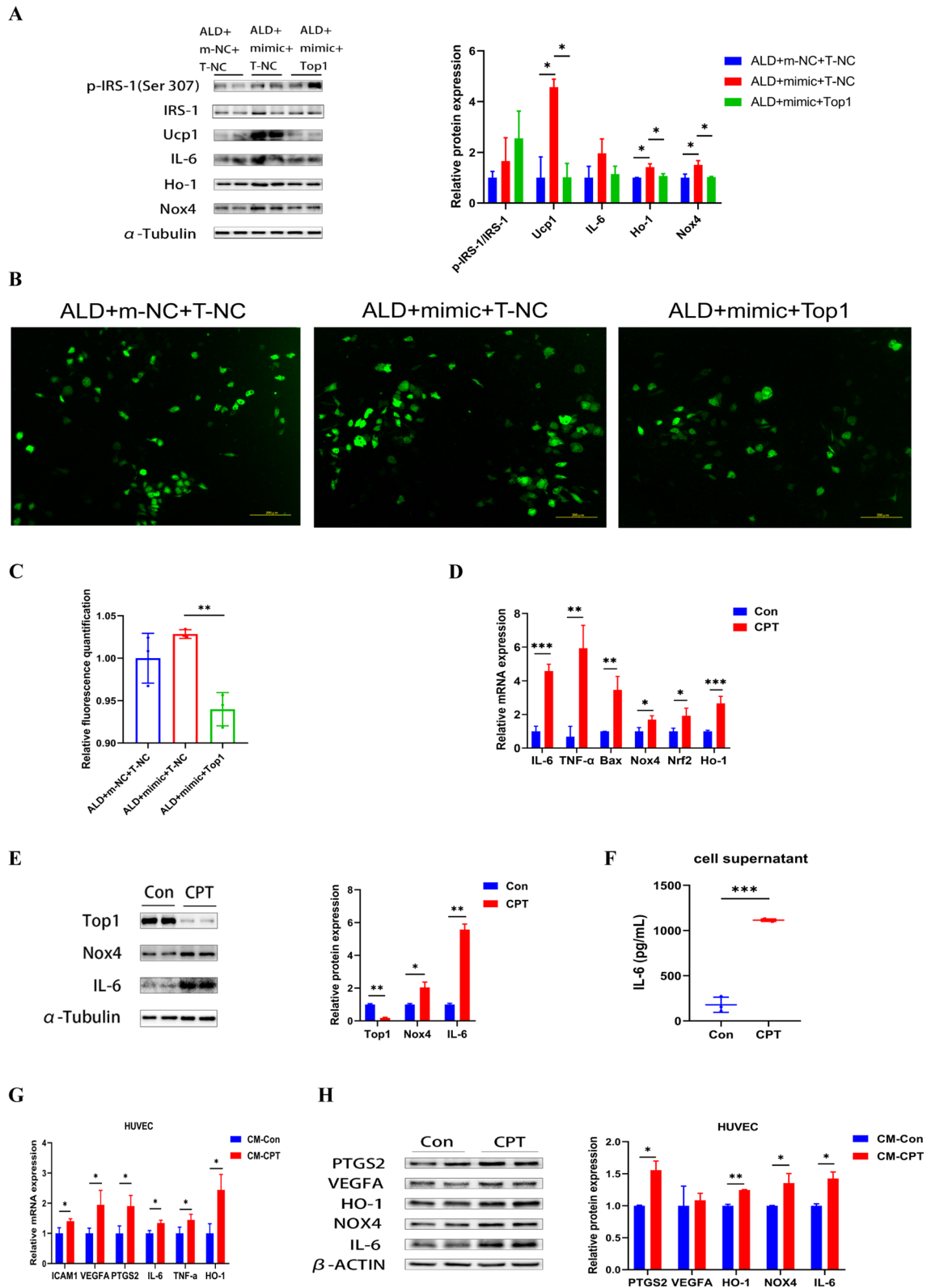


Fig. 6 (See legend on previous page.)

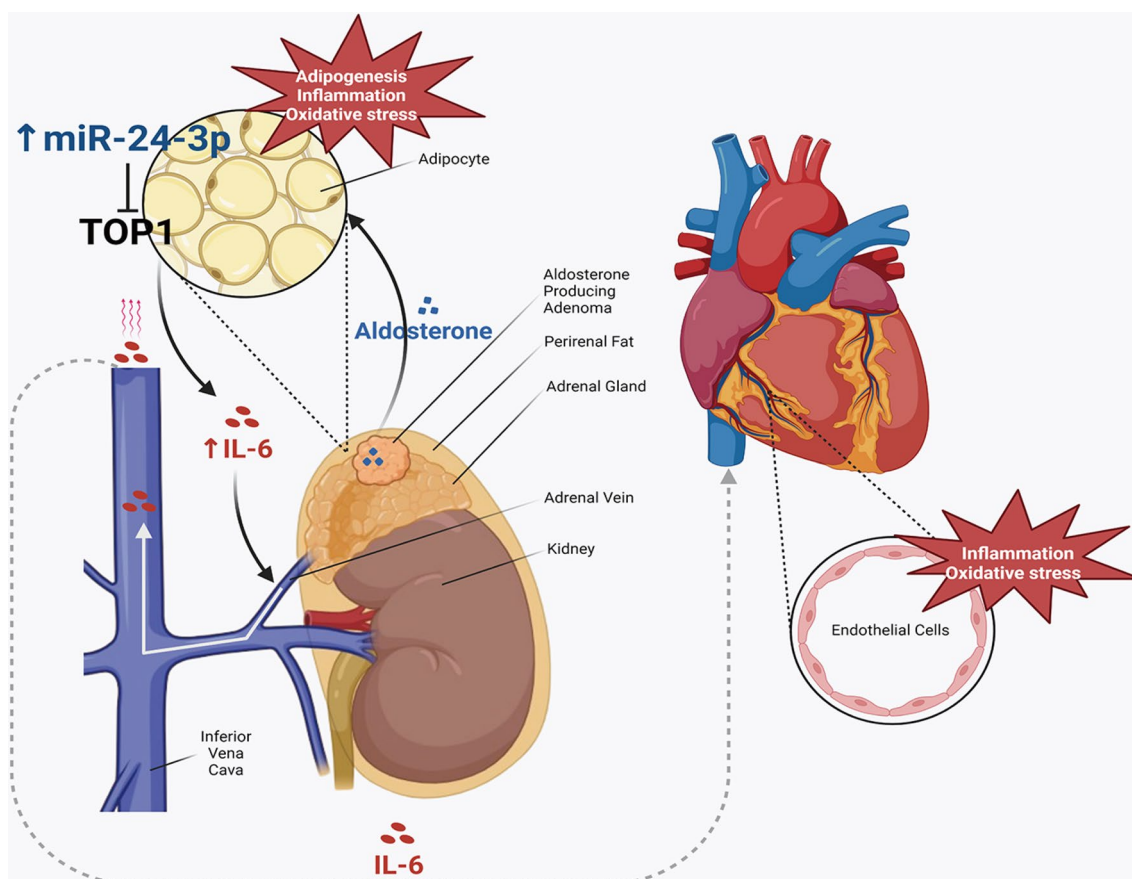


Fig. 7 Proposed mechanism of miR-24-3p/Top1 in the regulation of adipose properties and CVD risk in PA

linked to an increased incidence of metabolic syndromes such as obesity in patients with PA [28]. In addition, the ROC curve of total PRFT in patients with PA with and without CVD was analyzed, revealing an AUC of 0.79 and an optimal cutoff value of 28.07 mm, which suggests PRFT as a biomarker for early CVD risk detection in patients with PA (see Supplementary material, Figure S2), although further validation with larger sample sizes and prospective cohorts will be required.

Aldosterone promotes adipogenesis [29, 30], induces inflammation [31, 32], inhibits insulin-induced glucose uptake, and influences the expression and secretion of serum adipokines such as IL-6, chemerin and apelin, which exacerbate inflammation, vascular dysfunction, and atherosclerosis by modulating the immune response, insulin sensitivity, lipid metabolism, and vascular function, ultimately accelerating metabolic dysfunction and the development of CVD [8]. These findings suggest that aldosterone may impact CVD and metabolic abnormalities through adipose tissues or adipokines [33]. In PA, excessive aldosterone may affect both mature adipocytes and the differentiation

of preadipocytes, altering perirenal fat properties. Our results indicated that aldosterone-induced changes in the adipocyte phenotype were consistent with previous reports, with upregulated miR-24-3p expression. RESCUE experiments confirmed that miR-24-3p inhibition could reverse the effects of aldosterone on adipocytes. Our study provides another important pathway by which aldosteronism induces inflammation and oxidative stress.

The crosstalk between adipocytes and vascular endothelial cells under excessive aldosterone may contribute to the high risk of CVD in patients with PA. We constructed an adipocyte-HUVEC unidirectional co-culture system. We avoided using commonly employed transwell bilayer chambers to prevent HUVEC-secreted small molecules from influencing adipocytes, ensuring accurate assessment of the effects of adipocytes on HUVEC. Several previous studies have highlighted interactions between adipocytes and HUVEC. Tang et al. demonstrated that co-culturing 3T3-L1 overexpressing miR-27b-3p with HUVEC upregulated inflammatory markers in HUVEC [34]. Lai et al. reported

that HUVEC enhanced the differentiation of co-cultured 3T3-L1 through VEGFR2 signaling [35]. Pourdashti et al. reported that hypoxia-treated adipocytes significantly increased HUVEC proliferation and tubule formation [36]. These studies suggest that the crosstalk between adipocytes and endothelial cells may play an important role in the high risk of CVD.

In this study, we further focused on Top1, the target gene of miR-24-3p, which encodes DNA topoisomerase I. The first topoisomerase inhibitor, CPT [37, 38], blocks topoisomerase repair, causing DNA damage [39]. CPT derivatives, such as topotecan and irinotecan, have been developed and are widely used in antitumor therapy [40–42]. Wan et al. treated the breast cancer cell line ZR-75-1 with topotecan, which significantly increased cellular inflammatory indices and the expression of cytokines such as IL-6 and TNF- α [18]. Similarly, Kitai et al. reported that supernatants from topotecan-stimulated mouse breast cancer cell line E0771 increased the production of pro-inflammatory cytokines IL-6, CXCL10, and interferon in mouse bone marrow dendritic cells [19]. In tumor cells, Top1 inhibition severely disrupts DNA replication and transcription, damages DNA, and releases inflammatory mediators, harming tumor cell survival. On the other hand, some researchers have suggested that Top1 inhibition during lethal inflammation can protect the organism. Rialdi et al. found that therapeutic inhibition of Top1 during severe infections prevents local and systemic tissue damage caused by excessive pro-inflammatory factor activation, as validated in cellular and mouse models [20]. Such damage may be more potent than that caused by pathogen infection and may become the direct cause of death [43]. For example, during the early COVID-19 outbreak, many critically ill patients died from cytokine storms triggered by severe viral infections [44, 45]. Similarly, Ho et al. reported that topotecan inhibited SARS-CoV-2-induced lethal inflammation in a hamster model [21], and Yang et al. suggested that Top1 inhibitors increased the production of the anti-inflammatory cytokine IL-10 in endotoxemic mice, significantly reducing mortality [22]. We believe that different modeling conditions lead to varying effects of Top1 inhibition. Our model mainly involves aldosterone-stimulated adipocytes, which do not belong to either of the two previously mentioned models, and their relationship with Top1 has not been reported. We found that Top1-inhibited adipocytes released more IL-6 and directly impaired the function of co-cultured HUVEC. These findings suggest that circulating inflammatory factors may originate mainly from localized inflammation in perirenal fat, potentially increasing the risk of CVD in patients with PA.

The present study has several limitations. First, perirenal fat surrounds the adrenal gland and most adrenal veins, while the superior and middle perinephric veins communicate with veins derived from the ipsilateral adrenal gland [46]. The adrenal venous blood drains from not only perinephric fat but also adrenal cortical cells [47, 48]. Second, our study focused on adipocytes and endothelial cells in co-culture experiments. However, cardiac tissue consists mainly of cardiomyocytes, fibroblasts, and endothelial cells, and CVD may involve heart impairment in addition to vascular dysfunction. To fully explore the influence of adipocytes on CVD risk, attention should also be given to cardiomyocytes and fibroblasts. Furthermore, we did not validate the role of aldosterone and miR-24-3p in adrenocortical cells, nor the effects of adrenocortical cells on CVD-related cells. Future studies should consider expanding the analysis to additional cellular models. Third, the lack of animal experiments is another limitation, as animal models are crucial for validating inter-organ crosstalk. The complex in vivo hormonal and cellular environment may significantly influence experimental outcomes, and animal models will be the focus of our subsequent research.

Conclusion

In conclusion, the upregulation of miR-24-3p in perirenal fat, which induces adipogenesis, inflammation, and oxidative stress by targeting Top1, may contribute to vascular endothelial damage and be involved in the high risk of CVD in patients with PA.

Abbreviations

PA	Primary aldosteronism
CVD	Cardiovascular diseases
miRNA	MicroRNA
PRFT	Perirenal fat thickness
CT	Computed tomography
PAC	Plasma aldosterone concentration
ALD	Aldosterone
Adipoq	Adiponectin
APA	Aldosterone-producing adenoma
Top1	DNA Topoisomerase I
AVS	Adrenal venous sampling
HUVEC	Human umbilical vein endothelial cell
qPCR	Quantitative PCR
ELISA	Enzyme linked immunosorbent assay
GSH	Reduced glutathione
ROS	Reactive oxygen species
C/EBP α	CCAAT enhancer binding protein alpha
PGC1 α	PPARG coactivator 1 alpha
UCP1	Uncoupling protein 1
NRF2	Nuclear factor erythroid 2-related factor 2
HO-1	Heme oxygenase 1
NOX4	NADPH oxidase 4
CM	Conditioned medium
CPT	Camptothecin

Supplementary Information

The online version contains supplementary material available at <https://doi.org/10.1186/s12967-025-06329-1>.

Supplementary Material 1

Acknowledgements

We are very grateful to Prof. Hongbin Zhang (Denmark), Prof. Yuhua Tseng (Joslin Diabetes Center, Harvard Medical School) and Prof. Huijie Zhang (Nanfeng Hospital).

Author contributions

MP-G: conceived, designed and supervised the research and revised the manuscript. XL-L: conceived, designed and conducted the experiments; collected and analyzed the data; and wrote the manuscript. ML and YM-Z: collected the serum and tissue samples and discussed the experiments. RY-Z: collected and analyzed the data; created visual representations of the data; and discussed the experiments. XC-L, YJ-D, WZ, and QJ-F: collected the serum and tissue samples; and discussed the experiments. The other authors collaborated on the data or sample collection and interpretation. All authors have provided final approval of the submitted version.

Funding

This work was supported by the National Natural Science Foundation of China (grant number: 82270858 and 82470869) and Guangdong Basic and Applied Basic Research Foundation (grant number: 2024A1515012925) to Dr. Meiping Guan.

Availability of data and materials

For ethical reasons, the clinical characteristics of patients are not publicly available but are available from the corresponding authors upon reasonable request. The remaining data are available within the article or supplementary information or are available from the corresponding authors upon request.

Declarations

Ethics approval and consent to participate

Our study was approved by the ethics committee of Southern Medical University, and written informed consent was obtained from all the patients (No: NFEC-2021-049).

Consent for publication

Not applicable.

Competing interests

The authors declare that they have no competing interests.

Author details

¹Department of Endocrinology and Metabolism, Nanfang Hospital, Southern Medical University, Guangzhou, Guangdong, China. ²Department of Endocrinology, Shenzhen Hospital, Southern Medical University, Shenzhen, China. ³Department of Laboratory Medicine, Nanfang Hospital, Southern Medical University, Guangzhou, Guangdong, China. ⁴Department of General Surgery, Nanfang Hospital, Southern Medical University, Guangzhou, Guangdong, China. ⁵Division of Urology, Nanfang Hospital, Southern Medical University, Guangzhou, Guangdong, China. ⁶Division of Vascular and Interventional Radiology, Nanfang Hospital, Southern Medical University, Guangzhou, Guangdong, China.

Received: 5 October 2024 Accepted: 1 March 2025

Published online: 18 March 2025

References

- Ekman N, Grossman AB, Dworakowska D. What we know about and what is new in primary aldosteronism. *Int J Mol Sci.* 2024;25(2):900.
- Byrd JB, Turcu AF, Auchus RJ. Primary aldosteronism: practical approach to diagnosis and management. *Circulation.* 2018;138(8):823–35.
- Milliez P, Girerd X, Plouin PF, Blacher J, Safar ME, Mourad JJ. Evidence for an increased rate of cardiovascular events in patients with primary aldosteronism. *J Am Coll Cardiol.* 2005;45(8):1243–8.
- Monticone S, Burrello J, Tizzani D, Bertello C, Viola A, Buffolo F, et al. Prevalence and clinical manifestations of primary aldosteronism encountered in primary care practice. *J Am Coll Cardiol.* 2017;69(14):1811–20.
- Chen YL, Chen CH, Xu TY, Xu JZ, Zhu LM, Li Y, et al. Non-invasive left ventricular pressure-strain loop study on cardiac fibrosis in primary aldosteronism: a comparative study with cardiac magnetic resonance imaging. *Hypertens Res.* 2024;47(2):445–54.
- Reincke M, Fischer E, Gerum S, Merkle K, Schulz S, Pallauf A, et al. Observational study mortality in treated primary aldosteronism: the German Conn's registry. *Hypertension.* 2012;60(3):618–24.
- Wu C, Zhang H, Zhang J, Xie C, Fan C, Zhang H, et al. Inflammation and fibrosis in perirenal adipose tissue of patients with aldosterone-producing adenoma. *Endocrinology.* 2018;159(1):227–37.
- Fuster JJ, Ouchi N, Gokce N, Walsh K. Obesity-induced changes in adipose tissue microenvironment and their impact on cardiovascular disease. *Circ Res.* 2016;118(11):1786–807.
- Huang N, Mao EW, Hou NN, Liu YP, Han F, Sun XD. Novel insight into perirenal adipose tissue: a neglected adipose depot linking cardiovascular and chronic kidney disease. *World J Diabetes.* 2020;11(4):115–25.
- Liu BX, Sun W, Kong XQ. Perirenal fat: a unique fat pad and potential target for cardiovascular disease. *Angiology.* 2019;70(7):584–93.
- Tombol Z, Turai PI, Decmann A, Igaz P. MicroRNAs and adrenocortical tumors: where do we stand on primary aldosteronism? *Horm Metab Res.* 2020;52(6):394–403.
- Seyhan AA. Trials and tribulations of MicroRNA therapeutics. *Int J Mol Sci.* 2024;25(3):1469.
- Shuster A, Atlas M, Pinthus JH, Mourtzakis M. The clinical importance of visceral adiposity: a critical review of methods for visceral adipose tissue analysis. *Br J Radiol.* 2012;85(1009):1–10.
- Robertson S, MacKenzie SM, Alvarez-Madrado S, Diver LA, Lin J, Stewart PM, et al. MicroRNA-24 is a novel regulator of aldosterone and cortisol production in the human adrenal cortex. *Hypertension.* 2013;62(3):572–8.
- Fiedler J, Jazbutyte V, Kirchmaier BC, Gupta SK, Lorenzen J, Hartmann D, et al. MicroRNA-24 regulates vascularity after myocardial infarction. *Circulation.* 2011;124(6):720–30.
- Xiang Y, Cheng J, Wang D, Hu X, Xie Y, Stitham J, et al. Hyperglycemia repression of miR-24 coordinately upregulates endothelial cell expression and secretion of von Willebrand factor. *Blood.* 2015;125(22):3377–87.
- Squillace N, Bresciani E, Torsello A, Bandera A, Sabbatini F, Giovannetti C, et al. Changes in subcutaneous adipose tissue microRNA expression in HIV-infected patients. *J Antimicrob Chemother.* 2014;69(11):3067–75.
- Wan S, Pestka S, Jubin RG, Lyu YL, Tsai YC, Liu LF. Chemotherapeutics and radiation stimulate MHC class I expression through elevated interferon-beta signaling in breast cancer cells. *PLoS ONE.* 2012;7(3): e32542.
- Kitai Y. Elucidation of the mechanism of topotecan-induced antitumor immune activation. *Yakugaku Zasshi.* 2022;142(9):911–6.
- Rialdi A, Campisi L, Zhao N, Lagda AC, Pietzsch C, Ho J, et al. Topoisomerase 1 inhibition suppresses inflammatory genes and protects from death by inflammation. *Science.* 2016;352(6289):d7993.
- Ho J, Mok BW, Campisi L, Jordan T, Yildiz S, Parameswaran S, et al. TOP1 inhibition therapy protects against SARS-CoV-2-induced lethal inflammation. *Cell.* 2021;184(10):2618–32.
- Yang N, Yue R, Ma J, Li W, Zhao Z, Li H, et al. Nitidine chloride exerts anti-inflammatory action by targeting Topoisomerase I and enhancing IL-10 production. *Pharmacol Res.* 2019;148: 104368.
- Funder JW, Carey RM, Mantero F, Murad MH, Reincke M, Shibata H, et al. The management of primary aldosteronism: case detection, diagnosis, and treatment: an endocrine society clinical practice guideline. *J Clin Endocrinol Metab.* 2016;101(5):1889–916.
- Monticone S, D'Ascenzo F, Moretti C, Williams TA, Veglio F, Gaita F, et al. Cardiovascular events and target organ damage in primary aldosteronism compared with essential hypertension: a systematic review and meta-analysis. *Lancet Diabetes Endocrinol.* 2018;6(1):41–50.

25. Chen X, Mao Y, Hu J, Han S, Gong L, Luo T, et al. Perirenal fat thickness is significantly associated with the risk for development of chronic kidney disease in patients with diabetes. *Diabetes*. 2021;70(10):2322–32.
26. Kang M, Yan LM, Li YM, Zhang WY, Wang H, Tang AZ, et al. Inhibitory effect of microRNA-24 on fatty acid-binding protein expression on 3T3-L1 adipocyte differentiation. *Genet Mol Res*. 2013;12(4):5267–77.
27. Jin M, Wu Y, Wang J, Chen J, Huang Y, Rao J, et al. MicroRNA-24 promotes 3T3-L1 adipocyte differentiation by directly targeting the MAPK7 signaling. *Biochem Biophys Res Commun*. 2016;474(1):76–82.
28. Rossi GP, Sechi LA, Giacchetti G, Ronconi V, Strazzullo P, Funder JW. Primary aldosteronism: cardiovascular, renal and metabolic implications. *Trends Endocrinol Metab*. 2008;19(3):88–90.
29. Martinez-Martinez E, Cachofeiro V, Rousseau E, Alvarez V, Calvier L, Fernandez-Celis A, et al. Interleukin-33/ST2 system attenuates aldosterone-induced adipogenesis and inflammation. *Mol Cell Endocrinol*. 2015;411:20–7.
30. Rondinone CM, Rodbard D, Baker ME. Aldosterone stimulated differentiation of mouse 3T3-L1 cells into adipocytes. *Endocrinology*. 1993;132(6):2421–6.
31. Guo C, Ricchiuti V, Lian BQ, Yao TM, Coutinho P, Romero JR, et al. Mineralocorticoid receptor blockade reverses obesity-related changes in expression of adiponectin, peroxisome proliferator-activated receptor-gamma, and proinflammatory adipokines. *Circulation*. 2008;117(17):2253–61.
32. Zhou R, Lin ZH, Jiang CS, Gong JX, Chen LL, Guo YW, et al. Marine natural product des-O-methylsalsidiplodin effectively lowers the blood glucose level in db/db mice via ameliorating inflammation. *Acta Pharmacol Sin*. 2013;34(10):1325–36.
33. Wada T, Ohshima S, Fujisawa E, Koya D, Tsuneki H, Sasaoka T. Aldosterone inhibits insulin-induced glucose uptake by degradation of insulin receptor substrate (IRS) 1 and IRS2 via a reactive oxygen species-mediated pathway in 3T3-L1 adipocytes. *Endocrinology*. 2009;150(4):1662–9.
34. Tang Y, Yang LJ, Liu H, Song YJ, Yang QQ, Liu Y, et al. Exosomal miR-27b-3p secreted by visceral adipocytes contributes to endothelial inflammation and atherogenesis. *Cell Rep*. 2023;42(1): 111948.
35. Lai N, Jayaraman A, Lee K. Enhanced proliferation of human umbilical vein endothelial cells and differentiation of 3T3-L1 adipocytes in coculture. *Tissue Eng Part A*. 2009;15(5):1053–61.
36. Pourdashti S, Faridi N, Yaghoobi H, Jalali MT, Soroush A, Bathaie SZ. Possible role of WNT10B in increased proliferation and tubule formation of human umbilical vein endothelial cell cultures treated with hypoxic conditioned medium from human adipocytes. *Biotech Histochem*. 2022;97(3):168–79.
37. Hsiang YH, Liu LF. Identification of mammalian DNA topoisomerase I as an intracellular target of the anticancer drug camptothecin. *Cancer Res*. 1988;48(7):1722–6.
38. Hsiang YH, Hertzberg R, Hecht S, Liu LF. Camptothecin induces protein-linked DNA breaks via mammalian DNA topoisomerase I. *J Biol Chem*. 1985;260(27):14873–8.
39. Pourquier P, Pommier Y. Topoisomerase I-mediated DNA damage. *Adv Cancer Res*. 2001;80:189–216.
40. Fuchs C, Mitchell EP, Hoff PM. Irinotecan in the treatment of colorectal cancer. *Cancer Treat Rev*. 2006;32(7):491–503.
41. Garst J. Topotecan: an evolving option in the treatment of relapsed small cell lung cancer. *Ther Clin Risk Manag*. 2007;3(6):1087–95.
42. Crul M. CKD-602. *Chong Kun Dang. Curr Opin Investig Drugs*. 2003;4(12):1455–9.
43. Dragomir MP, Knutsen E, Calin GA. SnapShot: unconventional miRNA functions. *Cell*. 2018;174(4):1038.
44. Zheng Y, Li Y, Li M, Wang R, Jiang Y, Zhao M, et al. COVID-19 cooling: nanostrategies targeting cytokine storm for controlling severe and critical symptoms. *Med Res Rev*. 2024;44(2):738–811.
45. Hao S, Ning K, Kuz CA, Xiong M, Zou W, Park SY, et al. SARS-CoV-2 infection of polarized human airway epithelium induces necroptosis that causes airway epithelial barrier dysfunction. *J Med Virol*. 2023;95(9): e29076.
46. Ochi A, Muro S, Adachi T, Akita K. Zoning inside the renal fascia: The anatomical relationship between the urinary system and perirenal fat. *Int J Urol*. 2020;27(7):625–33.
47. Path G, Bornstein SR, Ehrhart-Bornstein M, Scherbaum WA. Interleukin-6 and the interleukin-6 receptor in the human adrenal gland: expression and effects on steroidogenesis. *J Clin Endocrinol Metab*. 1997;82(7):2343–9.
48. Willenberg HS, Path G, Vogeli TA, Scherbaum WA, Bornstein SR. Role of interleukin-6 in stress response in normal and tumorous adrenal cells and during chronic inflammation. *Ann NY Acad Sci*. 2002;966:304–14.

Publisher's Note

Springer Nature remains neutral with regard to jurisdictional claims in published maps and institutional affiliations.